Are high-T_c cuprates unusual metals?

1998 J. Phys.: Condens. Matter 10 11365

(http://iopscience.iop.org/0953-8984/10/49/024)

J. Phys.: Condens. Matter **10** (1998) 11365–11384. Printed in the UK PII: S0953-8984(98)98778-1

Are high-T_c cuprates unusual metals?

W Y Liang

IRC in Superconductivity and Cavendish Laboratory, Madingley Road, Cambridge CB3 0HE, UK

Received 29 October 1998

Abstract. The unusual properties of high-temperature superconductors are reviewed. The structure and chemistry of the materials are described and the strong influence of the carrier concentration on their superconducting properties is illustrated. The temperature dependences of the resistivity, Hall effects and thermoelectric power coefficients are given. These properties distinguish the cuprates clearly from any ordinary metal known until recently. In particular the normal Boltzmann transport theory is no longer applicable. It was found that these anomalous properties of the normal phase are accompanied by superconducting order parameters of uncommon symmetry (d wave), as well as non-BCS temperature and magnetic field dependences. The observation of the normal-phase pseudogap in the density-of-states spectrum by means of specific heat and other measurements seems to offer an important way forward in understanding both the normal phase and the high-temperature superconductivity mechanism.

1. Introduction

While the discovery of superconductivity in La–Ba–Cu–O ten years ago (Bednorz and Müller 1986) was undoubtedly one of the most remarkable scientific breakthroughs for over half a century, its impact upon the world of science and technology has proved to be far beyond the confines of the new superconductors. For the discovery not only took us to a hitherto unscaled height in superconducting transition temperature compared with the previously held record of 23.4 K observed for Nb_3Ge, but also it introduced an entirely new class of solids to physics and materials science. These new solids are full of surprises and set new challenges to our understanding of strongly correlated many-body problems, as well as new ways of exploiting them for technology. They have also been responsible for generating many diverse theoretical models in recent years. In other words, what was previously regarded as a secured knowledge of solids is now no longer adequate, neither in predicting this new phenomenon, nor in providing a satisfactory explanation for the unusual behaviour of high-temperature cuprate superconductors in both the normal and superconducting phases. Other than the high transition temperature, their unusual features include the simultaneous existence of superconductivity and low density of carriers, the departure from Fermi-liquid behaviour and, for the first time, crystallinity as a prerequisite for the metallic and superconducting characteristics. The crystal structures are two dimensional and contain CuO_2 layers as the conducting sheets. Although angle-resolved photoemission spectroscopy (ARPES) measurements suggest a $\boldsymbol{k}$-dependent Fermi surface (Marshall *et al* 1996), no convincing magnetic oscillations evidence from de Haas–van Alphen experiments has yet been found despite the gallant attempts at Los Alamos Laboratory employing explosives to produce high magnetic fields (Smith *et al* 1990) as well as the use of a more conventional

0953-8984/98/4911365+20$19.50

pulsed high-field magnet at Tohoku University (Kido *et al* 1990). This is surprising since there are very high-quality cuprate superconductors now available, e.g., of overdoped Tl-2201 ($T_c \sim 18$ K), with a long mean free path (>1000 Å at 1 K). It is also found that many of the important electronic properties of cuprate superconductors obey simple universal functions of reduced temperature, field, pressure or carrier density, all of which are dictated by the chemical doping, with faint regard to any subtle changes in the Fermi surface.

On examining the electronic properties of the cuprates, it is immediately clear that the origin of the unusual and intriguing behaviour is the strong Coulomb and exchange–correlation effects. With the Cu ions in the d^9 state, the cuprate has an odd number of electrons in its upper valence band. Instead of this leading to half-filling and a metal, however, an antiferromagnetic insulator is formed. At the same time, the magnetic correlation length is of the order of a few atomic distances, and as the superconducting carriers are introduced by chemical doping their density remains low with a degenerate temperature of only 10 to 20 times T_c. At such a low doping level, the high-T_c superconductor behaves much like a charged Bose liquid. However, as more carriers are added, the material becomes in many respects like a Fermi liquid. Over the years, considerable theoretical debate has concentrated on the question of the crossover between a Bose–Einstein condensate and a Fermi-liquid-based BCS superconductor, with as yet no clear consensus emerging as regards a correct description that covers the entire superconducting state. High-temperature superconductors thus behave in a peculiarly non-Fermi-surface-specific way and many conventional Fermi-liquid behaviours have become blurred in this system. We will show that these unusual behaviours are manifested in the superconducting as well as the normal phase.

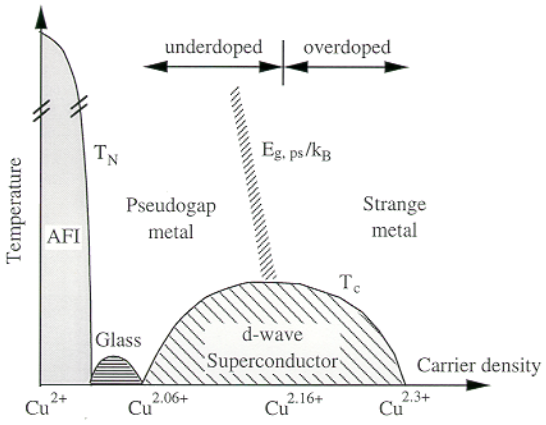

Figure 1. A generic critical-temperature–carrier-density phase diagram of high-T_c cuprate superconductors: zero carrier density corresponds to a Cu valence of 2+ in the CuO_2 layers.

Figure 1 shows a generic electronic phase diagram of cuprate superconductor. The antiferromagnetic Mott insulator phase is found near the origin where Cu in the CuO_2 layers is in the d^9 state (Cu valence = 2+ as in La_2CuO_4). This magnetic state is gradually destroyed by increased chemical doping, e.g., by the substitution of Sr^{2+} for La^{3+}, with a complete loss of the long-range antiferromagnetic order occurring at around 0.03 carriers per Cu ion ($Cu^{2.03+}$), which is followed by a spin-glass phase over a small range of doping (0.03–0.06). At about 0.055 carriers per Cu ion, the material undergoes an insulator-to-metal transition, at the same time displaying superconductivity at low temperature. The

superconductivity at this stage is weak with very small condensation energy and is unable to sustain appreciable critical current density particularly in a magnetic field. With further doping, T_c increases and reaches a maximum at about 0.16 carriers per Cu ion; thereupon T_c falls continuously to zero at 0.25–0.30 carriers per Cu ion. No superconductivity has been observed at higher doping and in any case the material often undergoes structural changes with large doping. Accordingly, in the superconducting domain, a cuprate may be classified as an underdoped or overdoped superconductor. The division into these two regimes turns out to be of some significance, whose origin has been the subject of much debate ever since high-temperature superconductivity became known.

Within the superconducting range, T_c varies universally and empirically as a parabolic function of the carrier density. In simple experimental terms, T_c in the underdoped regime appears to follow the prediction of a Bose–Einstein condensate with particle pairings occurring in real space and T_c increasing in a polynomial form of the carrier density (Uemura 1991) which also appears to be thermally activated. On the other hand, the overdoped regime bears many of the signatures of a BCS-type superconductor. We will show later that some of the above observations can be explained by the presence of pseudogaps in the normal phase. We will also argue that the physically significant critical value for the carrier density is that at which the pseudogap enters the phase diagram and not that at which T_c is maximum, and that the same should hold for the division between the so-called overdoped and underdoped regimes.

2. High-temperature superconductor families

2.1. The structure

There are well over one hundred different compounds that are high-T_c superconductors discovered in the past decade. All of them are formed in two-dimensional structures consisting of various metal oxide layers (except for the layers of Y, rare-earth elements

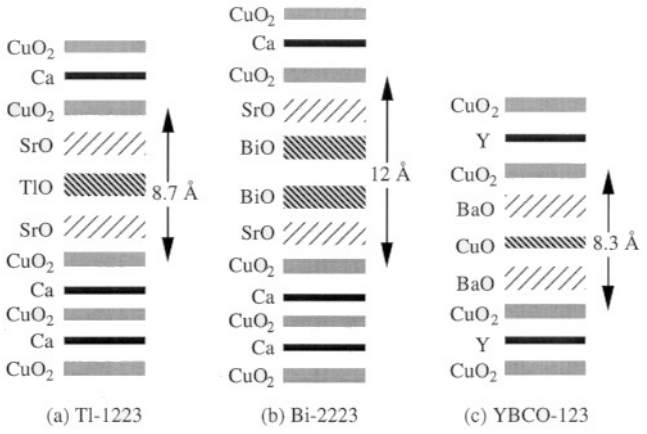

Figure 2. A schematic structural diagram of three major high-temperature superconducting families, each consisting of alternating two-dimensional layers of conducting CuO_2 and charge reservoir layers. The distance between adjacent CuO_2 layers has an important influence on the two-dimensional characteristics of the superconductor. In these examples, YBCO and Tl-1223 behave as anisotropic three-dimensional superconductors, while Bi-2223 behaves as a two-dimensional superconductor.

and Ca, which have no oxygen); some examples are shown schematically in figure 2. They share a common feature of the presence of one or more CuO_2 layers separated by layers containing mixed-valence metal oxides such as TlO–(Ba, Sr)O (figure 2(a)), BiO–SrO (figure 2(b)), CuO–BaO (figure 2(c)) and others such as HgO–BaO and (La, Sr)–O (not shown). The CuO_2 layers are responsible for the superconductivity while the mixed-valence metal oxide layers are the charge reservoir layers supplying mobile carriers to the CuO_2 layers. In addition, charge reservoir layers have different thicknesses causing widely varying degrees of anisotropy. Their presence weakens the electronic coupling between the superconducting layers and thus reduces the critical currents across the layers. These charge reservoir layers are therefore sometimes also called the blocking layers.

Table 1. (a) Hole-doped and (b) electron-doped homologous series ($n = 1, 2, 3, \ldots$) of high-T_c superconductors. The electron-doped materials usually require high pressure to synthesize.

	Remarks on properties
(a) Hole-doped compounds	
$La_{2-x}Sr_xCuO_4$	Related to the first high-T_c material discovered; $T_c \sim 38$ K; it remains a model high-T_c material due to its simple structure.
$CuBa_2(Ca, Y)_{n-1}Cu_nO_{2n+3}$; $Cu_2Ba_2(Ca, Y)_{n-1}Cu_nO_{n+4}$	$YBa_2Cu_3O_{7-\delta}$ (123) is the most researched material; $T_c \sim 93$ K; Y can be replaced by most rare earths. Granularity limits the critical current in the ceramic form. However, the problem can be avoided in large pseudo-single crystals—promising for magnetic bearing applications.
$(Bi, Pb)_2Sr_2Ca_{n-1}Cu_nO_{2n+4}$ $(Tl, Pb)_2Ba_2Ca_{n-1}Cu_nO_{2n+4}$	Bi-2223 has been the most popular candidate for tape applications; problems of weak pinning due to two dimensionality, and toxicity in the case of thallium.
$(Tl, Pb)_1Ba_2Ca_{n-1}Cu_nO_{2n+3}$	Tl-1223 is also a promising candidate for tapes but suffers from the same problem of granular weak links as YBCO in addition to showing Tl toxicity.
$(Hg, Pb)Ba_2Ca_{n-1}Cu_nO_{2n+2}$	Hg-1223 has the highest T_c (134 K under ambient pressure and 164 K at 200 kbar); problems of chemical stability and Hg toxicity reduce appeal. Doping with Re greatly enhances the irreversibility field.
(b) Electron-doped compounds	
$(Nd, Ce)_2CuO_4$	$T_c \sim 30$ K; it has a similar structure to $La_{2-x}Sr_xCuO_4$.
$(Sr, Ca)CuO_2$	$T_c \sim 110$ K; it has the simplest structure but the superconducting form is very difficult to fabricate.

2.2. The main families

Cuprate superconductors are most commonly named according to the number of mixed-valence metal oxide layers. For example, Bi-2223 and Tl-2201 have two Bi–O and two Tl–O layers respectively in the blocking layers (Tl-1201 has one Tl–O layer). The more common cuprates are listed in table 1 which includes both hole-doped materials (a) and electron-doped materials (b), as well as a summary of some of the more salient properties and technical problems associated with them.

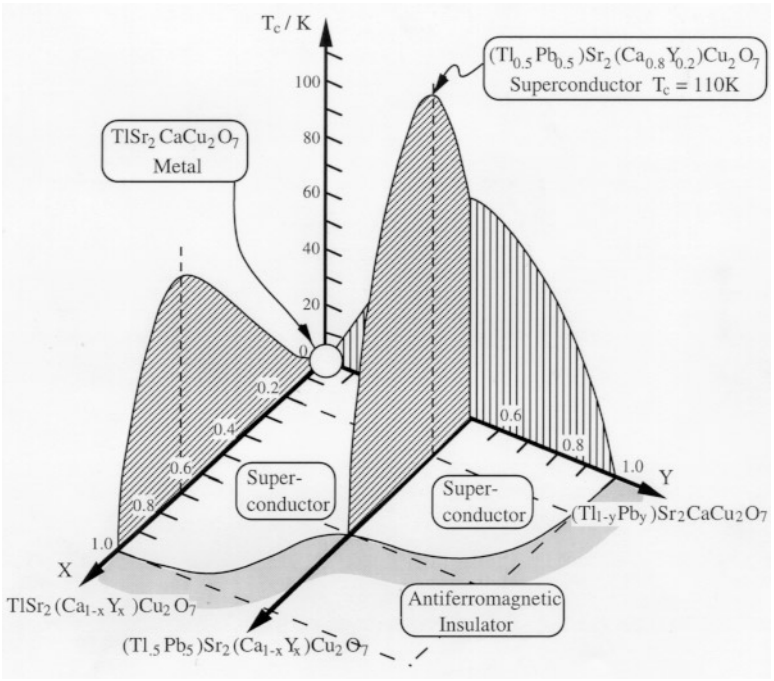

Figure 3. The metal–superconductor–insulator transmutation as seen in the series of compounds of the $(Tl, Pb)Sr_2(Ca, Y)Cu_2O_7$ family (Liu *et al* 1990).

2.3. Doping and superconductivity

As the parent form of each cuprate is an insulator, chemical doping is a necessary step for providing carriers. This can be accomplished by substituting for a cation element (not Cu) another element of different valency, or by changing the oxygen content. In fact, both methods are frequently used in the study of the effects of doping on high-temperature superconductivity. A most remarkable example of how chemical substitutions can lead to a series of metal–superconductor–insulator transmutation is shown in figure 3 for the $(Tl, Pb)Sr_2(Ca, Y)Cu_2O_7$ family (Liu *et al* 1990). Within this family of compounds, $TlSr_2CaCu_2O_7$ is a metal without superconductivity. Its Cu valence is 2.5+, but on reducing this to 2+ the compounds $PbSr_2CaCu_2O_7$ and $TlSr_2YCu_2O_7$ result, which are insulators. In between these limits, superconductivity prevails, each branch displaying a maximum T_c with an appropriate doping composition. Finally, by suitably adjusting the content of all six cation elements, we obtain a superconductor $(Tl_{0.5}Pb_{0.5})Sr_2(Ca_{0.8}Y_{0.2})Cu_2O_7$ with $T_c = 110$ K. It should be stressed that substitution for Cu in the CuO_2 layer with any other element introduces unwanted magnetic pair-breaking scattering, which invariably leads to a rapid destruction of the superconductivity.

2.4. d-wave superconductivity

In addition to a high value of T_c and a large superconducting energy gap, the cuprates are characterized by d-wave symmetry of their superconducting order parameters, particularly the energy gap, with interesting consequences for tunnelling and microwave properties. The reader is referred to the definitive experiments by Tsuei and Kirtley (1997) and Wollman

et al (1995) which verified this symmetry by the methods of pair tunnelling and half-integer flux quantization, and SQUID interferometry respectively. Recently, ARPES and penetration depth measurements have demonstrated that the energy gap has a more complex angular dependence than simply line nodes along the diagonals of the Brillouin zone of the *ab*-plane for the underdoped cuprates (Harris *et al* 1996, Ding *et al* 1996, Panagopoulos and Xiang 1998). Writing the energy gap as $\Delta_k(\phi) = \Delta_0|\cos 2\phi|$, where $\phi = 0$ along the $(\pi, 0)$ axis, these experiments show that the amplitude function Δ_0 has an additional ϕ-dependence, $\Delta_0 \equiv \Delta_0(\phi)$, such that the maximum amplitude lies in the $(\pi, 0)$ direction and the minimum in the (π, π) direction $(\phi = \pi/4)$.

3. Normal-state properties

In this section, we concentrate on the unusual aspects of normal-state properties that include the temperature dependences of the resistivity, Hall coefficients and thermoelectric power. The pseudogap phenomenon as observed in specific heat measurements is described separately in section 4.

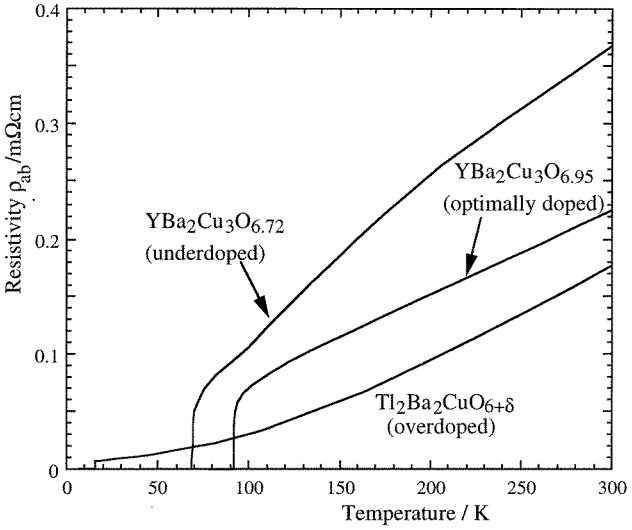

Figure 4. Typical temperature dependences of $\rho_{ab}(T)$ for underdoped ($YBa_2Cu_3O_{6.72}$), optimally doped ($YBa_2Cu_3O_{6.95}$) and overdoped ($Tl_2Ba_2CuO_{6+\delta}$) cuprates in zero field (Carrington *et al* 1993, Tyler *et al* 1998).

3.1. The temperature dependence of the resistivity

In general the resistivity $\rho(T)$ is such that

(i) the in-plane resistivity $\rho_{ab}(T)$ has a linear or quasi-linear temperature-dependent metallic-like behaviour at high temperature except for the extremely underdoped cuprates,
(ii) the out-of-plane resistivity $\rho_c(T)$ shows an activated semiconductor-like behaviour for all underdoped cuprates, and
(iii) $\rho_{ab}(T)$ continues rising at very high temperature, well beyond the Mott–Ioffe–Regel limit.

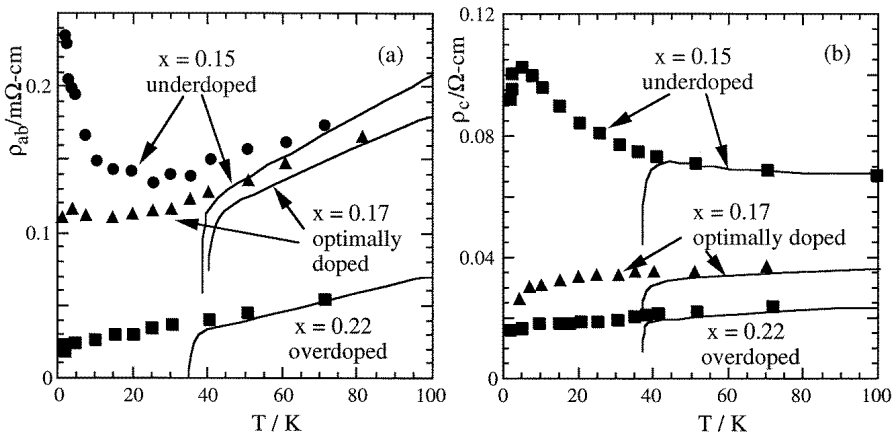

Figure 5. The resistivity of $La_{2-x}Sr_xCuO_4$ in a 60 T magnetic field and at low temperature: (a) $\rho_{ab}(T)$ and (b) $\rho_c(T)$, for the underdoped ($x = 0.15$), optimally doped ($x = 0.17$) and overdoped ($x = 0.22$) regimes; continuous curves show the resistivity in zero field (after Boebinger *et al* 1996).

These are useful but oversimplistic descriptions. The planar resistivity $\rho_{ab}(T)$ is linear with temperature only when the material is optimally doped to give the maximum T_c; otherwise there is a positive curvature when it is overdoped and a negative one when it is underdoped, as shown by the examples in figure 4 (Carrington *et al* 1993, Tyler *et al* 1998). These unusual characteristics become even more apparent when the temperature dependence of the Hall concentration is taken into account (see section 3.2). Figure 5 shows representative resistivity curves of $La_{2-x}Sr_xCuO_4$. They reveal 'normal' behaviour at very low temperature with a magnetic field of 60 T employed in the measurements (Boebinger *et al* 1996). Despite the considerable magnetoresistive effects, it is nevertheless clear that both $\rho_{ab}(T)$ and $\rho_c(T)$ show semiconductor-like behaviour in the underdoped regime ($x = 0.15$), with the semiconductor-to-metallic transition occurring just above optimal doping ($x = 0.17$). These measurements also show that even for materials having linear resistivity–temperature dependence above T_c in zero field, characteristic semiconducting behaviour can appear in the 'normal' resistivity at low temperature once the superconductivity has been removed by high magnetic field. It is this aspect which sometimes makes it very difficult to decide when a metal is truly a metal.

For certain cuprates which are chemically stable, it is useful to probe the resistivity to very high temperature, in particular at temperatures beyond the point where the mean free path, as given by the Boltzmann transport theory, has decreased to the value of the interatomic distance, known as the Mott–Ioffe–Regel limit. The resistivity of $(La_{1.85}Sr_{0.15})CuO_{4-\delta}$ is shown in figure 6 (Gurvitch and Fiory 1987). The fact that $\rho(T)$ continues to rise and remains practically linear well beyond the M–I–R limit is surprising and suggests that the usual Boltzmann transport theory for a well-defined Fermi surface has broken down. Furthermore, it is in fact non-trivial to explain what appears to be the same mechanism operating from 30 K to near the melting temperature of 1100 K. However, since similar results have also been observed for Sr_2RuO_4 superconductor (Tyler 1997), this transport mechanism may be a property that is not peculiar to the cuprates alone but is generally shared by all oxide metals.

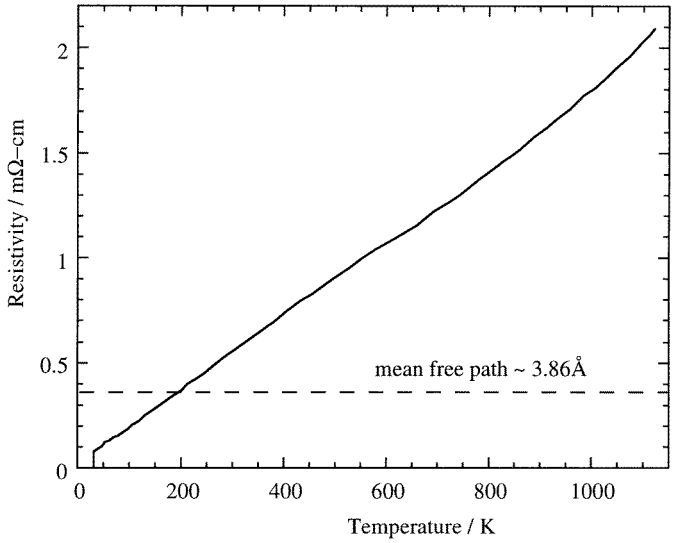

Figure 6. The resistivity of $(La_{1.85}Sr_{0.15})CuO_{4-\delta}$ at high temperature showing the persistence of the quasi-linear dependence well beyond the Mott–Ioffe–Regel limit (after Gurvitch and Fiory 1987).

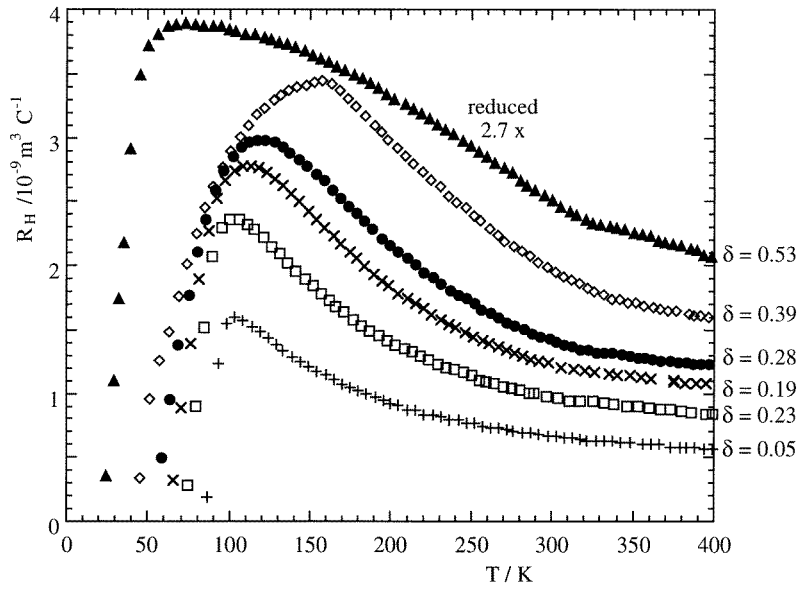

Figure 7. The temperature dependence of R_H for epitaxially grown films of $YBCO_{7-\delta}$ with $\boldsymbol{I} \parallel ab$-plane and $\boldsymbol{H}(7\ \mathrm{T}) \parallel \boldsymbol{c}$, $\delta = 0.05, 0.19, 0.23, 0.28, 0.39, 0.53$ (Carrington *et al* 1993).

3.2. The Hall coefficient

The Hall coefficient R_H shows for most cuprates a considerable temperature dependence throughout the whole of the doping range, although this dependence becomes weak for the highly overdoped samples. In general, R_H follows $1/T$ at high temperature and T

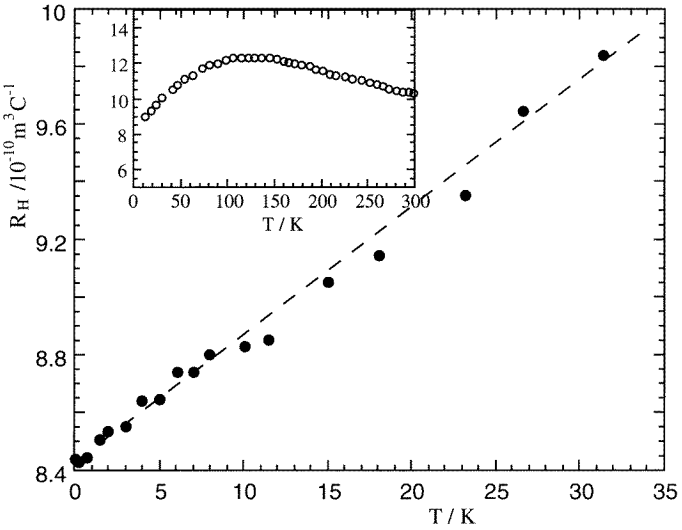

Figure 8. $R_H(T)$ at low temperature for an overdoped Tl-2201 single crystal measured in a 16 T magnetic field with $\boldsymbol{I} \parallel ab$-plane and $\boldsymbol{H}$(16 T) $\parallel c$-axis (the dashed line is a guide to the eye); the inset shows R_H at higher temperature (Mackenzie *et al* 1996).

at low temperature, with a maximum between these two regimes, as shown in figure 7 (Carrington *et al* 1993). Mackenzie *et al* (1996) extended the measurements of R_H (at 16 T) for an overdoped Tl-2201 single crystal to very low temperature and found that the linear temperature dependence persisted into the mK range as shown in figure 8. Although various models have been proposed to explain this Hall behaviour, including different carrier masses and various scattering lifetimes, truly convincing explanations have yet to be found. It is nevertheless interesting to note that if a simple one-band model is used, the R_H-values for Tl-2201 convert to (6–7) $\times$ 10^{21} carriers cm^{-3} at these temperatures, implying approximately one carrier per Cu ion.

3.3. The thermoelectric power

Classically, for a metal or a semi-metal, the thermoelectric power coefficient is strongly influenced by the velocity of the electron states at the Fermi level averaged over the whole of the Fermi surface and is therefore expected to vary according to the compound. The thermoelectric power of a hole-doped cuprate, however, is totally insensitive to the individual Fermi surface and varies in a systematic manner according to the carrier concentration. It has large positive values in the underdoped range and negative values in the overdoped range at room temperature, with the optimal doping being just positive, as shown in figure 9 for representative members of the cuprate family of figure 3 (Cooper and Carrington 1993). The highly systematic behaviour has been used very effectively as a guide for searching for samples with optimal doping. Additionally, because measurements of thermoelectric power are free from grain boundary effects, they can be made with a much greater consistency, providing further universal appeal.

A further remarkable property of the thermoelectric power of the cuprates is that, to a good approximation, its absolute values appear to be only a function of doping concentration and are independent of the differences that exist in different compounds as seen in figure 10,

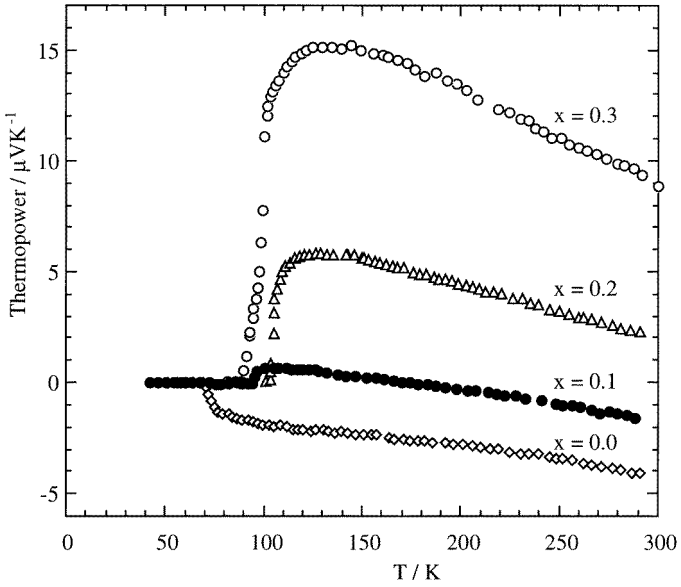

Figure 9. The temperature dependence of the thermoelectric power for some of the compounds $(Tl_{0.5}Pb_{0.5})Sr_2(Ca_{1-x}Y_x)Cu_2O_7$ $(0 \leqslant x \leqslant 0.3)$ (Cooper and Carrington 1993).

after Obertelli *et al* (1992). These results demonstrate that approximately the same absolute thermoelectric powers have been observed in a variety of samples at the underdoped limit (a), the maximum T_c (b) and near the overdoped limit (c), respectively.

4. The pseudogap phenomenon

4.1. Profiling low-lying states

Energy states within a few k_BT of the Fermi level will influence most strongly the transport and thermal properties. In addition to the various important energy parameters such as the superconducting energy gap ($\Delta_0 \sim 40$ meV), the exchange energy ($J \sim 130$ meV) and a typical phonon energy ($\hbar\omega \sim 60$ meV), the Fermi energy E_F of a cuprate superconductor has also been estimated to be as low as 150–250 meV. The comparability of these energies suggests the possibility of a strong-correlation effect and this is what makes the cuprates so interesting. One manifestation of the strong correlation is the appearance of pseudogaps at E_F in the normal phase. Experimentally, investigations of the nature of the low-lying states (close to E_F) are therefore of considerable value. We present here measurements of the specific heat providing information about all low-lying excitations including spin and charge degrees of freedom, averaging over all qs. In particular, we give evidence for the existence of pseudogaps in the normal phase, which is a highly unusual property for a superconductor and also clearly vital to understanding the superconductivity of the cuprates. Previously, the pseudogap phenomenon has been observed in measurements of bulk susceptibility (Alloul 1991), NMR Knight shift and relaxation rates (Takigawa *et al* 1989, 1991, Walstedt and Warren 1990) and inelastic neutron scattering (Rossat-Mignod *et al* 1992), all of which reflect a gap in the spin spectrum. Gap-like features have also been invoked to explain the deviation from linearity of the resistivity curves of underdoped

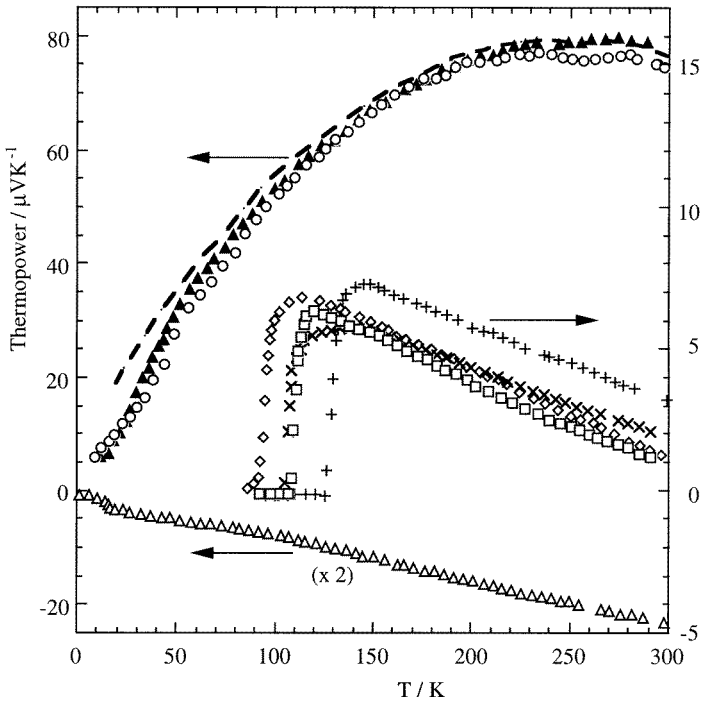

Figure 10. Plots of absolute values of the thermoelectric power as a function of temperature for a variety of samples at: (a) their underdoped limit (left-hand scale): ○, $YBa_2Cu_3O_{6.36}$; ▲, $(Tl_{0.5}Pb_{0.5})Sr_2(Y_{0.6}Ca_{0.4})Cu_2O_7$; - - - -, $Bi_2Sr_2(Y_{0.47}Ca_{0.53})Cu_2O_8$ single crystal; (b) optimal doping (right-hand scale): ◇, Bi-2212; ×, $(Tl_{0.5}Pb_{0.5})Sr_2(Y_{0.2}Ca_{0.8})Cu_2O_7$; □, Bi-2223; +, Tl-2223; and (c) their overdoped limit (left-hand scale): Δ, Tl-2201 (after Obertelli *et al* 1992).

cuprates (Uchida 1993, Cooper and Loram 1996) and the suppression at low frequencies of the in-plane scattering rate in the infrared reflectivity (Homes *et al* 1993, Basov *et al* 1995). Specific heat data for mainly underdoped $YBa_2Cu_3O_{7-\delta}$ ($0.8 \geqslant \delta \geqslant 0.03$), $La_{2-x}Sr_xCuO_4$ and $Y_{0.8}Ca_{0.2}Ba_2Cu_3O_{7-\delta}$ have also been reported (Loram *et al* 1993, Liang *et al* 1996, Loram *et al* 1998). It should be noted that quantitative information on the relative contributions of spin and charge excitations deduced from these measurements, for example from the specific heat and Pauli spin susceptibility, can serve as a useful test for several rival theoretical models for cuprate superconductors. We will concentrate on the $Y_{0.8}Ca_{0.2}Ba_2Cu_3O_{6+x}$ family because in this system we can investigate the full range of the superconducting phase domain from underdoped, through optimally doped, to overdoped superconductors by varying the oxygen concentration x.

4.2. The specific heat

An anomaly in the specific heat/temperature spectrum is associated with a thermodynamic phase transition. The transition between the superconducting and the normal phase will therefore give rise to such an anomaly. From the position of the anomaly therefore, T_c can be determined. The functional dependence of the electronic specific heat coefficient $\gamma^{el}(T)(=C^{el}(T)/T)$ not only gives a powerful indicator of any departure from simple metallic behaviour (linear in T), but for a superconductor below T_c, can also provide

evidence for pairing symmetry (an exponential function for s-wave symmetry and a polynomial for d-wave symmetry). The entropy function S^{el} can be deduced from the γ^{el}-spectrum:

$$S^{el}(T) = \int_0^T \gamma^{el}(T')\ \mathrm{d}T'$$

giving the number of thermal excitations (in units of k_B) in the energy range $|E-\mu| < 2k_BT$, where μ is the chemical potential ($\sim E_F$). An accurate measure of the entropy spectrum can provide useful quantitative information such as the integrated spectral weight near E_F. Integrating $S_n^{el} - S_s^{el}$ between T and T_c gives the thermodynamic free-energy difference between the normal and the superconducting phases:

$$F_n - F_s = H_c^2(T)/8\pi$$

where $H_c^2 \sim H_{c1}H_{c2}$ is the thermodynamic critical field, while the integration from $T = 0$ to T_c gives the superconducting condensation energy $U(0)$:

$$U(0) = \int_0^{T_c} (C_n^{el} - C_s^{el})\ \mathrm{d}T = H_c^2(0)/8\pi.$$

The number of condensed pairs can be estimated from $U(0)/\Delta(0)$ and the coherence volume can be obtained from an analysis of either Gaussian or critical fluctuations close to T_c. It is useful to remember that for a BCS superconductor, the condensation energy $U(0)$ can be obtained approximately from the anomaly jump, $T_c\,\Delta C(T_c)/4$ or $T_c^2\,\Delta\gamma^{el}(T_c)/4$. Conversely, these relationships may be used to test how well the Fermi-liquid description applies to the cuprates. We note also that the function $S^{el}(T)/T$ gives a very good measure of the electronic density-of-states function $g(E = k_BT)$ in the neighbourhood of E_F.

4.3. Specific heat experiments

Accuracy in the electronic specific heat measurements is of paramount importance, but achieving this has long posed a formidable experimental challenge because the electronic specific heat is smaller than the phonon specific heat by about two orders of magnitude, except at very low temperature. These phonon terms will therefore need to be carefully 'subtracted' from the 'total' specific heat to yield the electronic component. This involves an accuracy of better than ~1:104 in all the measurements in order to ensure an ~1% accuracy in the resultant electronic spectrum, and such a level of precision has been achieved by Loram (1983) who successfully carried out the measurement of changes in the electronic specific heat as a function of doping by employing the following procedure:

(i) a differential technique and an appropriate choice of reference sample remove directly at least 94% of the phonon terms;
(ii) the residual correction is made in subsequent computations of the raw data by approximating to a series of Einstein specific heat functions which scale linearly in magnitude with doping.

The choice of the reference sample is crucial and it should be used throughout the whole series of measurements. Ideally it should be structurally identical to the superconductor (having the same symmetry and containing atoms of closely similar atomic masses in the unit cell) but should not superconduct. Such a reference sample usually belongs to the same family as the superconductor under investigation but has been doped to remove its superconducting properties. For example, the insulating end member $YBCO_6$ or the non-superconducting $YBa_2(Zn_xCu_{1-x})_3O_{7-\delta}$ (where $x = 2$ or 7%) could be the appropriate reference for studying the electronic specific heat of $YBCO_{7-\delta}$.

This procedure has proved to be satisfactory through extensive checking for internal consistency. A maximum systematic uncertainty of about 10% in the electronic entropy S^{el} has been achieved for a realistic 1–2% uncertainty in the phonon specific heat contribution. Overall, the largest uncertainty in the electronic specific heat coefficient γ^{el} $(=C^{el}/T)$ is probably to be found at around 40 K. It is believed that the maximum error in γ^{el} is always less than 0.3 mJ K^{-2}/gram atom. The experimental accuracy was further improved as the series of measurements were carried out using one sample, whose oxygen content was varied by annealing the same sample at different temperatures and under different oxygen pressures. The value of δ was accurate to 0.01 according to direct measurements of the weight loss (mass of sample: ∼4.0 g) relative to the smallest δ-value (0.03) which had been calibrated by the neutron refinement technique.

4.4. $Y_{0.8}Ca_{0.2}Ba_2Cu_3O_{6+x}$

We reported the observation of a pseudogap in the $YBa_2Cu_3O_{7-\delta}$ system (Loram *et al* 1993, Liang *et al* 1996). However, since optimal doping occurs near full oxygenation ($YBCO_{6.93}$) this system provides only the possibility of probing mainly the underdoped range. Close to the fully oxygenated $YBCO_7$, a series of complex changes in the electronic as well as structural properties take place. It is probable that the disorder in the CuO chains due to the introduction of oxygen vacancies is causing a disproportionately large effect, which may complicate the specific heat results. This problem can be avoided in Ca-doped YBCO which has a substantial disorder built in throughout. Substituting Ca^{2+} for Y^{3+} adds holes to the CuO_2 planes and this in turn lowers the oxygen content required to give maximum T_c. For 20% Ca this optimal oxygen content is reduced to $O_{6.68}$, thus allowing both overdoped ($>O_{6.68}$) and underdoped ($<O_{6.68}$) regimes of the YBCO system to be studied. However, this amount of Ca substitution puts the antiferromagnetic insulating state beyond reach since even with the lowest oxygen content ($<O_{6.3}$), YBCO(20% Ca) remains metallic and weakly superconducting with $T_c \sim 40$ K. After removing from the raw data a low-temperature anomaly due to an extrinsic effect of magnetic origin which is oxygen independent and therefore does not affect relative changes in $\gamma(T)$ with x, the results of the specific heat measurements on $Y_{0.8}Ca_{0.2}Ba_2Cu_3O_{6+x}$ are as presented in figures 11(a)–11(d).

Figures 11(a) and 11(b) show a striking contrast in the behaviour of $\gamma^{el}(T)$ between the two regimes. In the overdoped regime ($x > 0.68$; figure 11(a)), the anomaly in the $\gamma^{el}(T)$ curves and T_c decrease gradually with increasing doping x, while $\gamma^{el}(0) = 0$ and γ_n remain substantially unchanged. However, in the underdoped regime ($x < 0.68$; figure 11(b)) there is a qualitatively different behaviour, namely, a rapidly diminishing anomaly height $\delta\gamma^{el}(T_c)$ accompanying a gradual decrease in T_c with decreasing doping x. Figures 11(c) and 11(d) provide further evidence of the fundamental differences already seen above. Over most of the overdoped regime, γ^{el}, S^{el} and S^{el}/T show behaviour typical of a conventional BCS metal. Here the normal-phase γ_n and S_n/T vary little with temperature or x, indicating that the electronic density-of-states function $\gamma_n(E)$ is only weakly energy and doping dependent with no unusual modification near E_F. However, starting from about $x = 0.73$, a little above x_{opt} (=0.68 for maximum T_c) and towards the underdoped regime, all of the above parameters change abruptly; particularly noticeable is the rapidly diminishing anomaly height, $\delta\gamma^{el}(T_c)$, as has been demonstrated already. A further decrease in x of ∼20% just below $x \sim 0.73$ (figure 11(b)) produces a decrease in $\delta\gamma^{el}(T_c)$ by a factor of five. These abrupt changes are the clearest experimental evidence for the appearance of pseudogaps accompanied by a loss of available states for electrons from the energy spectrum around E_F in the underdoped regime. We note that a careful examination of the critical oxygen

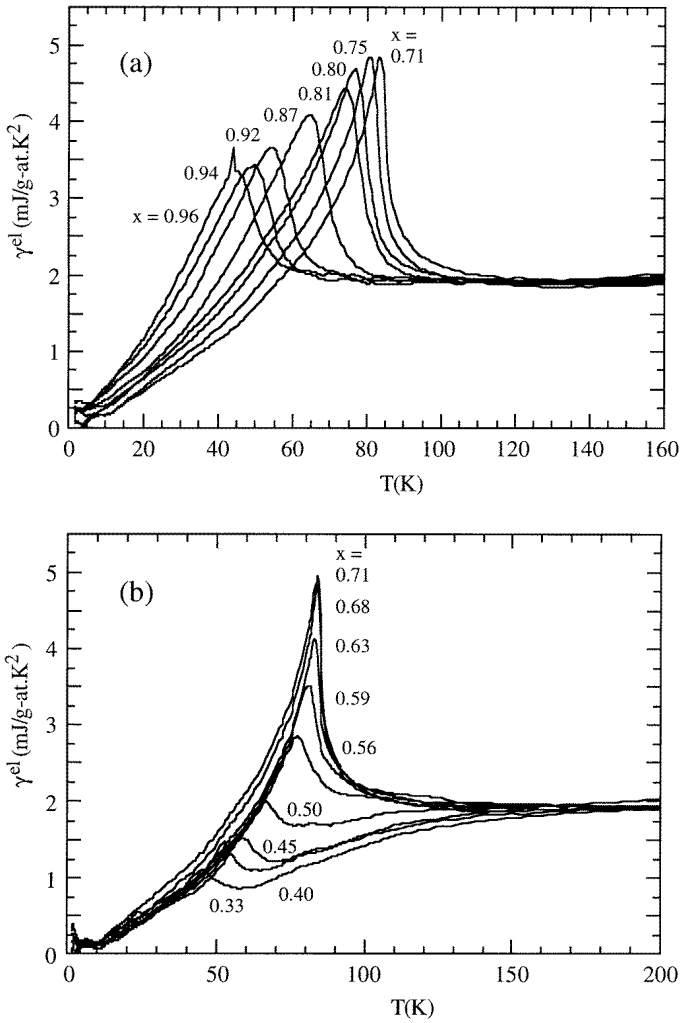

Figure 11. Specific heat results for $Y_{0.8}Ca_{0.2}Ba_2Cu_3O_{6+x}$ as functions of temperature plotted for a series of oxygen contents x: (a) $\gamma^{el}(T)$ for the overdoped regime ($x > 0.68$); (b) $\gamma^{el}(T)$ for the underdoped regime ($x < 0.68$); (c) $S^{el}(T)$ for both overdoped and underdoped regimes; (d) $S^{el}(T)/T$ also for the overdoped and underdoped regimes. The dashed curves ($x = 0.68$) represent optimal doping for maximum T_c.

concentration for the appearance of the pseudogap shows that $x_{crit} \sim 0.77$, a result to which we will return in section 4.6.

Above 200 K, γ_n^{el} changes very little across the entire doping range. The appearance of the pseudogap for $x < x_{crit}$ not only causes a sharp reduction of the superconductivity anomaly heights, $\delta\gamma^{el}(T_c)$, but also shifts the entropy curves S_n^{el} in the normal phase downwards (figure 11(c)). While for $x > x_{crit}$, all of the S_n^{el}-curves extrapolate to the origin, this downward shift, which increases as the pseudogap becomes bigger, produces a negative entropy intercept at 0 K. This negative intercept provides a means of quantifying the loss of entropy and therefore available states. The fact that the entropy loss is not restored at high temperature suggests that changes in the pseudogap with x are not

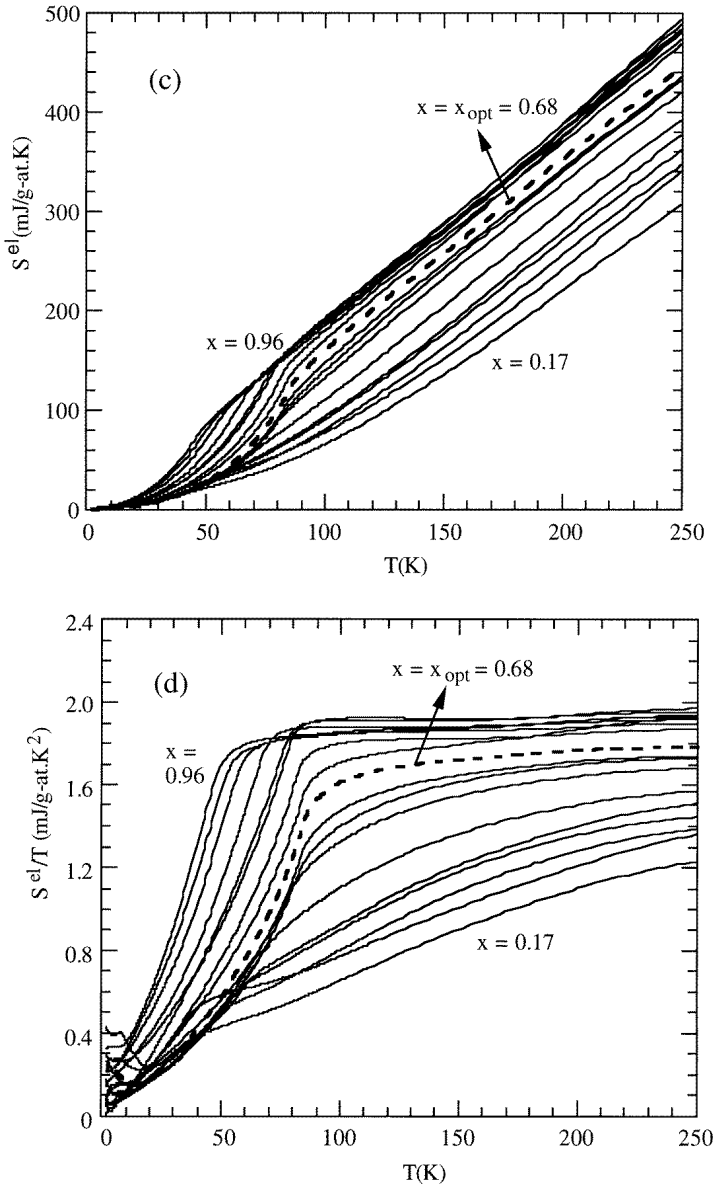

Figure 11. (Continued)

accompanied by a redistribution of states, but involve a direct addition or subtraction of one orbital/doped hole to the density-of-states curve on the flanks of the pseudogap. On the basis of the linear change of $S_n^{el}(280\ \mathrm{K})$ with x, which has slope $= 0.53k_B$/formula unit $= 0.38(k_B \ln 4)$/formula unit, it is estimated that 0.38 holes are given to the double CuO_2 layers for one oxygen atom added. A similar value was found for $YBCO_{6+x}$ (Loram *et al* 1998).

The variations in T_c, the condensation energy $U(0)$ and the quantity $U(0)/T_c^2\gamma_n^{el}$, where $\gamma_n^{el} \equiv \gamma^{el}(300\ \mathrm{K})$, as functions of x are given in figure 12. T_c varies more or less

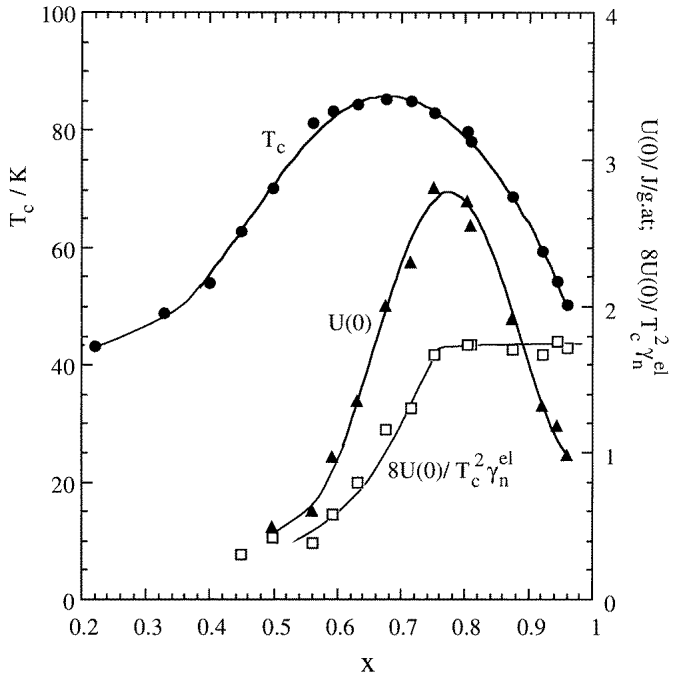

Figure 12. Variations in T_c, the condensation energy $U(0)$ and the quantity $U(0)/T_c^2\gamma_n^{el}$ as functions of x for $Y_{0.8}Ca_{0.2}Ba_2Cu_3O_{6+x}$, where $\gamma_n^{el} = \gamma^{el}(300\ \mathrm{K})$.

symmetrically with doping about a broad maximum at $x = x_{opt} = 0.68$. In contrast, the condensation energy $U(0)$ has a sharp maximum situated at $x = x_{crit} \sim 0.77$. At the same time, a plot of $U(0)/T_c^2\gamma_n^{el}$ shows that this quantity remains constant ($\sim$0.2) on the overdoped side, suggesting that the decrease in $U(0)$ here is conventional and is consistent with that expected for a gapless density of states. Only the fall in $U(0)$ in the underdoped regime is anomalous due to the opening of the pseudogap. It is interesting to note that changes in these thermodynamic parameters have apparently not been affected by the presence of disorder in the CuO chains, probably because the degree of disorder has remained constant throughout the doping range.

Finally, Loram *et al* (1998) claimed that as x falls in the underdoped regime, the superconducting gap $\Delta_0(0)$ increases monotonically while T_c falls to zero. This gives rise to an increasing gap ratio $2\Delta_0(0)/k_BT_c$ in the pseudogap region while the same ratio remains constant ($\sim$5.3 to 6) in the metallic overdoped region. On the other hand, penetration depth experiments give a different result, which suggests that $2\Delta_0(0)/k_BT_c$ is constant throughout the whole doping range (Panagopoulos and Xiang 1998). The disagreement may be due to the fact that specific heat experiments measure the amplitude of the gap parameter $\Delta_0(\phi)$ (as in $\Delta(\phi) = \Delta_0(\phi)|\cos 2\phi|$) averaged over all ϕs while penetration depth experiments are most sensitive to the amplitude close to the line nodes (π, π). There is little doubt, however, that the normal-state pseudogap, e.g., opens abruptly at $x \sim x_{crit}$ and grows with decreasing x; e.g. becomes comparable with k_BT_c at the optimum doping, $x = x_{opt} = 0.68$. Since $\Delta_0(0)$ and $\gamma_n^{el}(300\ \mathrm{K})$ remained large in the underdoped regime, Loram *et al* (1998) concluded that the growth of the pseudogap with decreasing x was responsible for the rapid weakening of the condensate and the rather slower decrease in T_c.

4.5. Characteristics of the pseudogap

The presence of pseudogaps in the underdoped range appears to be a universal feature for all cuprate superconductors. It should be noted that the pseudogap evolves when holes are removed from the underdoped cuprate; this is accompanied by the loss of a corresponding number of hole states from the density-of-states function within $E_F \pm E_{g0}$, while the density-of-states function is elsewhere kept unchanged. This contrasts strongly with the process of removing impurity carriers from a heavily doped semiconductor (i.e., making it less metallic). In this case, holes or electrons are removed from existing orbitals in the valence or conduction band. The process in the cuprates implies that the change in the spectral weight with doping does not occur at E_F but instead is distributed within the pseudogap such that the latter retains a quasi-triangular shape until it closes at the critical hole concentration. Such a triangle-shaped gap is consistent with the $\boldsymbol{k}$-space symmetry of d waves, as for the superconducting gap in cuprates. The pseudogap model of Loram *et al* (1998) is therefore

$$E_g(\phi, x) = E_{g0}(x)|\cos 2\phi|.$$

To a first approximation, we may view the local density-of-states function in $\boldsymbol{k}$-space, $g(E, \phi)$, as a square-well function whose width varies linearly from 0 at $\phi = \pi/4$ to $E_{g0}(x)$ at $\phi = 0$; doping merely changes the size of $E_{g0}(x)$. These authors also interpret the doping dependence of the pseudogap in terms of the kinetic energy E_{KE} of non-interacting holes as

$$E_{g0}(x) \sim J' - E_{KE}(x)$$

where $J' \sim$ 1000–1500 K and is clearly related to the in-plane exchange energy $J \sim$ 130 meV, strongly suggesting that scattering of the Cu spins on this energy scale may be responsible for the existence of the pseudogap, at least in the region of small x. This also lends weight to the argument that when holes are added, the new orbitals are located predominantly in the regions of maximum gap ($\phi = 0, \pi/2$ etc) in $\boldsymbol{k}$-space where spin–spin scattering is strongest. The pseudogap phase is therefore given by $E_{KE}(x) < J'$, and the pseudogap energy $E_{g0}(x)$ of correlated holes and spins softens towards the chemical potential as $E_{KE}(x)$ increases. At the same time, by considering the entropy as determined by specific heat measurements and comparing with the Pauli spin susceptibility, Loram *et al* (1993) concluded that the pseudogap is present for both charge and spin excitations and cannot be attributed solely to a gap in the spin spectrum or to a spinon gap.

A transition from semiconductor-like behaviour to strongly correlated-metal behaviour occurs at $x = x_{crit}$ when $E_{g0}(x_{crit}) = 0$. For $x > x_{crit}$, the entropy in the normal phase, S_n^{el} (above T_c; figure 11(d)), has no temperature dependence and, at the same time, $2\Delta_0(0)$ scales with $k_B T_c$ and $U(0)$ with $\gamma_n^{el} T_c^2$ (figure 12), both confirming the Fermi-liquid scenario and the absence of the normal-state pseudogap in the overdoped regime.

4.6. Criticality of the carrier concentration

In $Y_{0.8}Ca_{0.2}Ba_2Cu_3O_{6+x}$, we have seen that the pseudogap opens abruptly at an oxygen concentration, $x_{crit} \sim 0.77$, just above that for maximum T_c, $x_{opt} = 0.68$. It is now more convenient to translate these x-values to the more general planar hole density based on the bond-valence-sums model (Tallon *et al* 1995), given as $p = 0.19(x + 0.27)$ for $x > 0.3$ in $Y_{0.8}Ca_{0.2}Ba_2Cu_3O_{6+x}$, where p is the number of holes per CuO_2 in the superconducting plane. The pseudogap expression then becomes

$$E_{g0}(p) = J'(1 - p/p_{crit}) \sim J' - E_{KE}(p)$$

and $p_{crit} \sim 0.19$, which is equally applicable to $YBa_2Cu_3O_{7-\delta}$, $Bi_2Sr_2CaCu_2O_{8+\delta}$, and to Sr-doped $La_{2-x}Sr_xCuO_4$ systems (Loram *et al* 1998).

It has been consistently observed that when T_c is at its maximum value, $p = p_{opt}$ which is close to p_{crit}, where the pseudogap closes. This suggests that $E_{KE}(p_{crit}) \sim J'$ is an important condition for strong superconductivity. The region between p_{crit} and p_{opt} is particularly interesting where the condensate energy $U(0)$ has the steepest rise for a small increase in p while T_c is falling. This rise in $U(0)$ may be associated with the fact that when the pseudogap $E_{g0}(p)$ becomes smaller than the superconducting gap $\Delta_0(0)$, the additional spectral weight due to doping falls wholly within the energy range $E_F \pm \Delta_0(0)$, feeding the superfluid density below T_c and enhancing superconductivity. As observed, this occurs within a narrow doping range $(p_{crit} - p)/p_{crit} \sim \Delta_0(0)/J' \sim 0.2$. It is interesting that this basic study now finds an important application in superconducting technology. The irreversibility field H_{irr} at a given temperature closely tracks the behaviour of the condensation energy $U(0)$ and peaks at $p = p_{crit}$ as demonstrated in figure 13 (Johnson *et al* 1998). For this stoichiometry of $(Y,Ca)Ba_2Cu_3O_{6+x}$, $x_{opt} \sim 0.6$ and $x_{crit} \sim 0.86$, figure 13 shows a strong irreversibility-field enhancement on making x close to x_{crit}. This emphasizes the importance of choosing x_{crit} rather than x_{opt} as the preferred doping concentration for practical high-current high-field applications of cuprate superconductors.

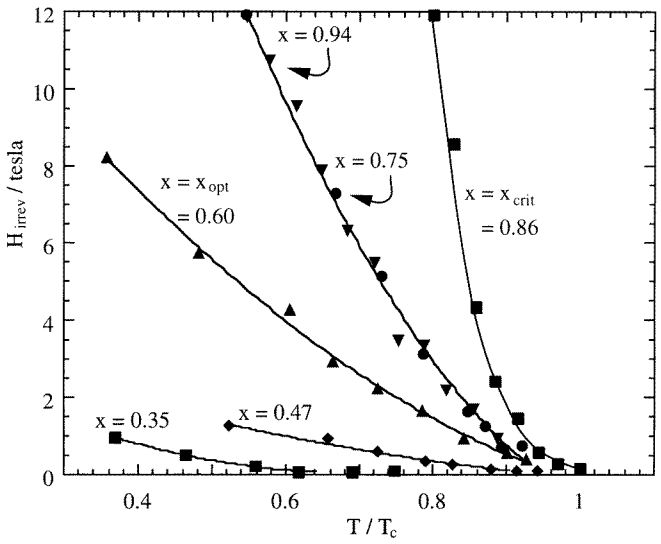

Figure 13. An irreversibility-field plot for Ca-doped $YBCO_{6+x}$ with varying oxygen concentration x. For this sample, $x_{opt} \sim 0.6$ (maximum T_c) and $x_{crit} \sim 0.86$ (maximum $U(0)$) (after Johnson *et al* 1998).

5. Conclusions

In this short review several examples have been given to demonstrate the unusual properties of high-T_c cuprates in their normal and superconducting phases. The origin of these characteristics must be the strong-correlation effects involving the spins of the Cu d^9 ions ($J_{exch} \sim 130$ meV) and the underlying doped charges in the CuO_2 layers of all high-T_c superconductors. From many experiments, there emerge highly systematic patterns with the

carrier (hole) concentration (p) being the dominant variable, which divides every system into the underdoped, optimally doped, critically doped and overdoped regimes. Optimal doping corresponds to maximum T_c whereas critical doping sets the scene for the creation of pseudogaps with a reduction of available one-electron states at the Fermi level, which rapidly depletes the strength of the superconductivity for $p < p_{crit}$. Thus although T_c varies relatively slowly with p with a broad maximum at $p = p_{opt} \sim 0.16$, the condensate energy $U(0)$, the associated superconducting free-energy difference and the technologically important parameter H_{irr} all maximize at $p = p_{crit} \sim 0.19$. This maximum is characterized by a sharp fall below p_{crit} due to the creation of the pseudogap and semi-metallic properties, but at the same time, a metallic behaviour above p_{crit}. These effects are all interrelated and account qualitatively for other anomalous properties of these materials.

The direct observation of pseudogaps in the cuprates is an important breakthrough. In addition to specific heat measurements, this is now supported by many other experiments, including ARPES, NMR Knight shift, susceptibility, tunnelling and Raman spectroscopy ones. These measurements show the absence of spin–charge separation, previously proposed as a possible mechanism for high-temperature superconductivity. The combined electronic specific heat and the spin-susceptibility analyses show that, as the carrier concentration is decreased below p_{crit}, the pseudogap removes one-electron states rather than redistribute them in the density-of-states spectrum. This indicates further that the pseudogap phenomenon does not originate from a Fermi-surface instability involving cooperative interactions such as spin- or charge-density waves or precursor superconducting fluctuations, but does point to the important role of incoherent scattering of charged carriers with Cu spins. These conclusions confirm that high-T_c cuprates are unusual metals with non-Fermi-liquid behaviour in the underdoped regime, transforming abruptly at $p = p_{crit}$ to basically Fermi-liquid phases in the overdoped regime; but these latter phases continue to be dominated by strong-correlation effects.

Acknowledgments

I like to thank J W Loram, J R Cooper and J D Johnson for providing me with their data, and A S Alexandrov, C Panagopoulos and C C Tsuei for many helpful discussions.

References

Alloul H 1991 *Physica* B **169** 51
Basov D N, Mook H A, Dabrowski B and Timusk T 1995 *Phys. Rev.* B **52** 13 141
Bednorz J G and Müller K A 1986 *Z. Phys.* B **64** 189
Boebinger G S, Ando Y, Passner A, Kimura T, Okuya M, Shimoyama J, Kishio K, Tamasaku K, Ichikawa N and Uchida S 1996 *Phys. Rev. Lett.* **77** 5417
Carrington A, Walker D J C, Mackenzie A P and Cooper J R 1993 *Phys. Rev.* B **48** 13 051
Cooper J R and Carrington 1993 *Adv. Supercond.* **5** 95
Cooper J R and Loram J W 1996 *J. Physique* **1** 6 2237
Ding H, Norman M R, Campuzano J C, Randeria M, Bellman A F, Yokoya T, Takahashi T, Mochiku T and Kadowaki K 1996 *Phys. Rev.* B **54** R9678
Gurvitch M and Fiory A T 1987 *Phys. Rev. Lett.* **59** 1337
Harris J M, Shen Z X, White P J, Marshall D S, Schabel M C, Eckstein J N and Bozovic I 1996 *Phys. Rev.* B **54** R15 665
Homes C C, Timusk T, Liang R, Bonn D A and Hardy W N 1993 *Phys. Rev. Lett.* **71** 1645
Johnson J D, Tallon J L, Williams G V M, Bernhard C, Pooke D M and Meinhold R H 1998 to be published
Kido G, Komorita K, Katayama-Yoshida H, Takahashi T, Kitaoka Y, Ishida K and Yoshitomi T 1990 *Adv. Supercond.* **3** 227

Liang W Y, Loram J W, Mirza K A, Athanassopoulou N and Cooper J R 1996 *Physica* C **263** 277
Liu R S, Edwards P P, Huang Y T, Wu S F and Wu P T 1990 *J. Solid State Chem.* **86** 334
Loram J W 1983 *J. Phys. E: Sci. Instrum.* **16** 367
Loram J W, Mirza K A, Cooper J R and Liang W Y 1993 *Phys. Rev. Lett.* **71** 1740
Loram J W, Mirza K A, Cooper J R and Tallon J L 1998 *J. Phys. Chem. Solids* at press
Mackenzie A P, Julian S R, Sinclair D C and Lin C T 1996 *Phys. Rev.* B **53** 5848
Marshall D S, Dessau D S, Loeser A G, Park C H, Matsuura A Y, Eckstein J N, Bozovic I, Fournier P, Kapitulnik A, Spicer W E and Shen Z X 1996 *Phys. Rev. Lett.* **76** 4841
Obertelli S D, Cooper J R and Tallon J L 1992 *Phys. Rev.* B **46** 14 928
Panagopoulos C and Xiang T 1998 *Phys. Rev. Lett.* **81** 2336
Rossat-Mignod J, Regnault L P, Bourges P, Vettier C, Burlet P and Henry J Y 1992 *Phys. Scr.* T **45** 74
Smith J L, Fowler C M, Freeman B L, Hults W L, King J C and Mueller F M 1990 *Adv. Supercond.* **3** 231
Takigawa M, Hammel P C, Heffner R H, Fisk Z, Smith J L and Schwarz R B 1989 *Phys. Rev.* B **39** 300
Takigawa M, Reyes A P, Hammel P C, Thompson J D, Heffner R H, Fisk Z and Ott K C 1991 *Phys. Rev.* B **43** 247
Tallon J L, Bernhard C, Shaked H, Hitterman R L and Jorgensen J D 1995 *Phys. Rev.* B **51** 12 911
Tsuei C C and Kirtley J R 1997 *Physica* C **282–287** 4
Tyler A W 1997 *PhD Dissertation* University of Cambridge
Tyler A W, Ando Y, Balakirev F F, Passner A, Boebinger G S, Schofield A J, Mackenzie A P and Laborde O 1998 *Phys. Rev.* B **57** R728
Uchida S 1993 *Japan. J. Appl. Phys.* **32** 3784
Uemura Y J 1991 *Nature* **352** 605
Walstedt R E and Warren Jr W W 1990 *Science* **248** 1082
Wollman D A, Van Harlingen D J, Giapintzakis J and Ginsberg D M 1995 *Phys. Rev. Lett.* **74** 797